RSC Advances

PAPER

View Article Online
View Journal | View Issue

Check for updates

Cite this: *RSC Adv.*, 2023, **13**, 12469

Isomerization and reaction process of $N_2O_4(H_2O)_n$

Yi Guo, [a] Zhiyong Huang,[a] Gan Tian,[a] Wei Wu,[b] Jie Lin[c] and Xinlong Chang*[a]

Liquid propellant N_2O_4 is prone to absorb H_2O to form an $N_2O_4(H_2O)_n$ system during long-term storage, ultimately generating HNO_3, HNO_2, and other substances capable of corroding the storage tank, which will adversely affect the performance of weapons and equipment. In this work, the reaction process of the $N_2O_4(H_2O)_n$ system is simulated using density functional theory, and the potential energy surface, the geometric configurations of the molecules, the charge distribution, and the bond parameters of the reaction course at $n = 0$–3 are analyzed. The results show that the potential energy of the system is lower and the structure is more stable when the H_2O in the $N_2O_4(H_2O)_n$ system is distributed on the same side. When $n = 1$ or 2, the reaction profiles are similar, and the systems are partly ionic, although still mainly covalently bonded. When $n = 3$, the charge on the *trans*-$ONONO_2$ group and the ON–ONO_2 bond length change abruptly to −0.503 a.u. and 2.57 Å, respectively, at which point the system is dominated by ionic bonds. At $n = 2$, a proton-transfer phenomenon occurs in the reaction course, with partial reverse charge-transfer from NO_3^- to NO^+, making the ON–ONO_2 bond less susceptible to cleavage, further verifying that $N_2O_4(H_2O)_n$ tends to afford the products directly in one step as H_2O accumulates in the system.

Received 7th March 2023
Accepted 3rd April 2023

DOI: 10.1039/d3ra01515g

rsc.li/rsc-advances

Open Access Article. Published on 21 April 2023. Downloaded on 12/6/2025 3:27:13 PM.
This article is licensed under a Creative Commons Attribution-NonCommercial 3.0 Unported Licence.

1 Introduction

Liquid-fuelled strategic missiles mainly use N_2O_4 and unsym-dimethylhydrazine (UDMH) as propellants, and during long-term storage, N_2O_4 as an oxidant will absorb moisture from the surrounding environment to produce an $N_2O_4(H_2O)_n$ system, ultimately generating HNO_3, HNO_2, and other corrosive substances, accelerating corrosion of the receptacle and potentially allowing propellants to leak.[1] Traditional liquid-fuelled strategic missiles are constrained by this factor and can only be temporarily refilled with N_2O_4 before launch to shorten the contact time between N_2O_4 and the receptacle, but this process leads to long preparation cycles and slow operational response of such missiles, to the detriment of their operational performance.

N_2O_4 is a volatile, reddish-brown transparent liquid at room temperature. It is a highly toxic chemical, which hampers experimental studies. N_2O_4, as a dimer of NO_2, is an important intermediate (IM) in the hydrolysis of NO_2 and plays an important role in the formation of acid rain.[2] Due to its noxious nature, the use of quantum calculations to probe the evolution of the $N_2O_4(H_2O)_n$ system is a trend of current research. Some studies have been carried out on the isomerization and self-ionization of N_2O_4 and the dimerization of NO_2, but the understanding of the chemical mechanism is still incomplete.[3–14] In particular, the effect of H_2O on the $N_2O_4(H_2O)_n$ system needs to be explored more deeply. Pimentel *et al.*[5] found that N_2O_4 isomerization and NO_2 dimerization in the presence of H_2O can directly form ONO–NO_2. Miller *et al.*[4] simulated the interaction of H_2O with ONO–NO_2 at room temperature. For the $N_2O_4(H_2O)_n$ system, the ionization rate is two orders of magnitude lower when $n = 1$ and 2 than when $n > 2$, indicating that, in the latter case, the reaction is transient and there is no IM. Medeiros *et al.*[6] mentioned that local minima for the $N_2O_4(H_2O)_n$ system can only be found when n is odd. Putikam *et al.*[9] found a "roaming-like" transition state f formed in ONO–NO_2 during the collision with H_2O by the stretching of the N–N bond and the rotation of the –NO_2 group. Finlayson-Pitts *et al.*[10] proposed a mechanism for the hydrolysis of N_2O_4:

$$2NO_2(g) \leftrightarrow N_2O_4(g) \quad (1)$$

$$N_2O_4(g) \leftrightarrow N_2O_4(surface) \quad (2)$$

$$N_2O_4(surface) \rightarrow ONONO_2(surface) \quad (3)$$

$$ONONO_2(surface) \rightarrow NO^+NO_3^-(surface) \quad (4)$$

$$NO^+NO_3^-(surface) + H_2O \rightarrow HONO(g) + HNO_3(surface) \quad (5)$$

N_2O_4 first forms *sym*-N_2O_4, which isomerizes to ONO–NO_2 and then reacts with H_2O to form HONO and HNO_3. The above hydrolysis mechanism reveals the complex diversity of species in the $N_2O_4(H_2O)_n$ system and the high number of isomers of

[a]*School of Missile Engineering, Rocket Force University of Engineering, Xi'an, 710025, China. E-mail: xinlongch@vip.sina.com*

[b]*Center of Engineering Quality Supervision, Logistics Support Department, Beijing, 100142, China*

[c]*School of Electronic Information and Communication, Huazhong University of Science and Technology, Wuhan, 430074, China*

© 2023 The Author(s). Published by the Royal Society of Chemistry

Open Access Article. Published on 21 April 2023. Downloaded on 12/6/2025 3:27:13 PM. This article is licensed under a Creative Commons Attribution-NonCommercial 3.0 Unported Licence.

N_2O_4.[3] The precise structures of the resulting HONO and HNO_3 after combining with H_2O remain uncertain.

In the propellant storage environment, N_2O_4 is distinct from that in the atmospheric environment and exists mainly in liquid form. The reaction profile of the $N_2O_4(H_2O)_n$ system after absorbing H_2O from air and forming the $N_2O_4(H_2O)_n$ system is unclear. Therefore, in this study, we have investigated the isomerization and reaction profile of the $N_2O_4(H_2O)_n$ system based on density functional theory (DFT), focusing on the following issues:

(1) The effects on the $N_2O_4(H_2O)_n$ system of n being an odd or even number.

(2) The route by which the $N_2O_4(H_2O)_n$ system directly forms NO^+ and NO_3^-.

(3) The variations in the charges on the groups during the reaction course of the $N_2O_4(H_2O)_n$ system when $n = 0$–3.

2 Calculation method

Based on the conclusions of Pimentel *et al.*,[5] the DFT/B3LYP method was used to optimize N_2O_4 single-molecule isomerization at the 6-311++G (3df, 2p) basis group level, considering all species in the reaction of the $N_2O_4(H_2O)_n$ system. The intrinsic reaction coordinates (IRC) were established through standard 6-311++G (3df, 2p) basis group calculations to confirm the connection of each transition state (TS) to the specified intermediate (IM). The resulting reactant, product, and IM frequencies were positive, with one and only one imaginary frequency for the TS. Single-point energies were re-determined at the B2PLYP/Def2-TZVP basis set level.[15] To take into account the effect of the solvent medium, the self-consistent reaction field (SCRF) method and the implicit solvation model of the SMD model were used at $n = 3$, in conjunction with the conclusions of Miller[4] and Putikam.[9] All calculations were performed using the Gaussian 16 software package.[16]

3 Results and discussion

3.1 Isomerization of N_2O_4 ($n = 0$)

Experimental studies have shown that N_2O_4 has three main conformations; in addition to *sym*-N_2O_4, there are two asymmetric N_2O_4 isomers, namely *trans*-N_2O_4 and *cis*-N_2O_4.[17–19] Zhu *et al.*[8] predicted the possible geometric conformations of N_2O_4 isomers based on *ab initio* molecular dynamics, and identified the most stable isomers as *sym*-N_2O_4 and *trans*-N_2O_4. Meanwhile, the spontaneous dissociation of N_2O_4 to NO_2 is less likely in the liquid propellant storage environment. Therefore, the work in this section mainly considers the mutual isomerization between *sym*-N_2O_4, *cis*-N_2O_4, and *trans*-N_2O_4. The potential energy surface (PES) and the geometric configurations and bond parameters of the conformers during the isomerization are shown in Fig. 1. The optimized *sym*-N_2O_4 has an N–N bond length of about 1.80 Å and N–O bond lengths of about 1.18 Å, in good agreement with reported values determined experimentally by electron diffraction analysis at 252 K.[20] When *sym*-N_2O_4 isomerizes to *cis*-N_2O_4, the N–N bond length in TS1 is 2.68 Å and the dihedral angle O4–N2–O6–N1 is 177°. The associated potential energy barrier is 166.91 kJ mol^{-1}, which further completes the isomerization process of NO_2 proposed by Liu *et al.*[3] In contrast, the "roaming-like" TS structure proposed by Putikam *et al.*[9] is more relaxed, with an N–N bond length of 3.70 Å, a dihedral angle O4–N2–O6–N1 of 76°, and a potential energy barrier of 34.31 kJ mol^{-1}, significantly different from the values calculated here. For the isomerization of *sym*-N_2O_4 to *trans*-N_2O_4 *via* TS3, the two –NO_2 groups of the reactants and products are coplanar, but the structure of TS3 is vertical, the N–N bond length is only 2.08 Å, and the associated potential energy barrier is about 175.94 kJ mol^{-1}. In contrast, in the TS structure reported in the literature, the N–N bond length reaches 3.57 Å, the two –NO_2 groups are almost dissociated, and the electron

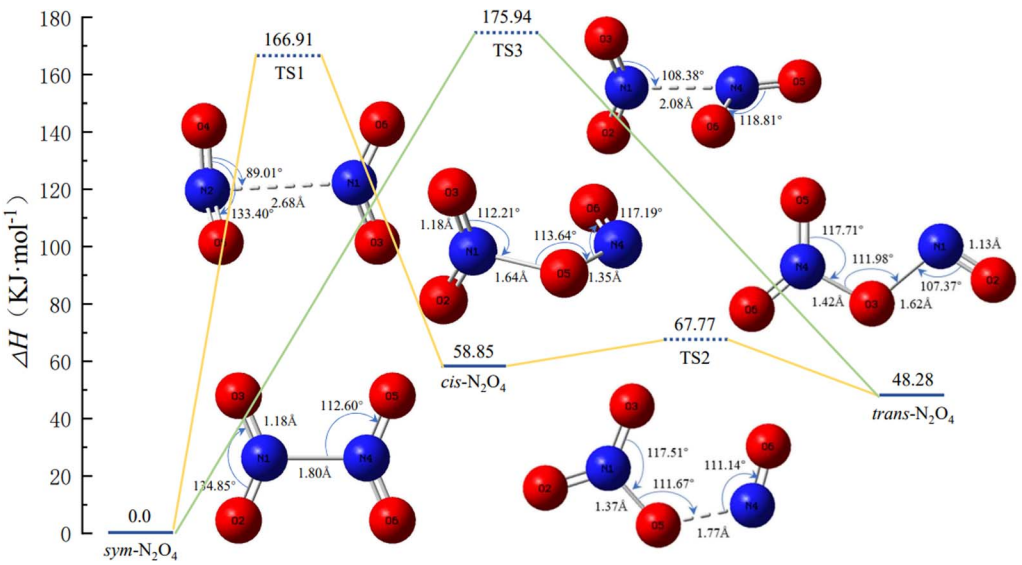

Fig. 1 Potential energy surface of N_2O_4 isomerization and the geometries and bond parameters of the conformers (key length unit: Å, key angle unit: °).

© 2023 The Author(s). Published by the Royal Society of Chemistry

Open Access Article. Published on 21 April 2023. Downloaded on 12/6/2025 3:27:13 PM.
This article is licensed under a Creative Commons Attribution-NonCommercial 3.0 Unported Licence.

density between the interacting groups is reduced, so the TS potential energy barrier (53.56 kJ mol^{-1}) is much lower than that calculated here.[9] The course of the isomerization of *cis*-N_2O_4 to *trans*-N_2O_4 is similar to that calculated in the literature.[21]

3.2 Isomerization and reaction processes of $N_2O_4(H_2O)$ and $N_2O_4(H_2O)_2$ (n = 1, 2)

From Section 3.1, it is clear that the relative energy of *trans*-N_2O_4 is lower than that of *cis*-N_2O_4, indicating that the former is more stable in the course of the isomerization. Hence, only *trans*-N_2O_4 is considered in the following calculations. Fig. 2 shows the PES and the geometric configurations of the molecules with bond parameters for the isomerization and reaction course of $N_2O_4(H_2O)$. When N_2O_4 absorbs H_2O, a complex such as IM1 is produced due to van der Waals forces. At this point, two pathways are available for IM1 for the next reaction step.

(1) IM1 may be directly converted to HNO_3 + *trans*-HONO *via* TS4, as shown in Fig. 2. TS4 is a compact five-membered-ring structure with an associated potential barrier of 138.62 kJ mol^{-1}. This value is similar to that reported by Chou *et al.*[22] Upon further conversion of TS4, H8 in H_2O gradually detaches and combines with one of the $-NO_2$ groups to produce *trans*-HONO. The remaining –OH of H_2O combines with the other $-NO_2$ group to produce HNO_3.

(2) IM1 may be converted to TS5 to generate *trans*-$ONONO_2$. In this case, the structure of TS5 is more similar to TS3. In the course of isomerization of *sym*-N_2O_4 to *trans*-N_2O_4, one of the $-NO_2$ groups rotates about the N–N bond, thus causing a shift of H_2O, and the distance between N1 and O7 reaches 4.02 Å. When structurally stable *trans*-$ONONO_2$ is generated, the distance between N1 and O7 is 2.85 Å. As the reaction continues, *trans*-$ONONO_2$ produces HNO_3 + *trans*-HONO and HNO_3 + *cis*-HONO through two six-membered-ring transition states, TS6 and TS7, respectively. In TS6, H8 of H_2O is transferred to O5 in $-NO_3$, eventually forming HNO_3, while the remaining –OH of H_2O combines with –NO. The structure of TS7 is similar to that of TS6, except that H_2O is rotated by a certain angle. It follows a similar reaction course to finally form HNO_3 + *cis*-HONO, the reaction potential of which is 2.41 kJ mol^{-1} higher than that of HNO_3 + *trans*-HONO.

In Fig. 2, it can be seen that the energy of *trans*-HONO is lower than that of *cis*-HONO, indicating that the former is more stable and the reaction pathway is more likely to occur. Therefore, the reaction course of *cis*-HONO is not considered in the following calculations. When the content of H_2O is further increased, N_2O_4 combines with more H_2O in the vicinity to produce $N_2O_4(H_2O)_2$. The PES and geometric configurations of the molecules with bond parameters for the isomerization and reaction course are shown in Fig. 3.

Similar to IM1 in Fig. 2, when N_2O_4 is combined with 2 H_2O, two $N_2O_4(H_2O)_2$ complexes, IM2 and IM3, are produced, as shown in Fig. 3(b), in which the 2 H_2O molecules are located on the same or opposite sides of N_2O_4, respectively. Therefore, its reaction course will follow two main pathways.

3.2.1 IM2 reaction process. ① IM2 is directly converted to TS12, from which HNO_3 + *trans*-HONO + H_2O are formed. TS12 has a five-membered-ring structure, similar to TS4, with only one H_2O molecule involved in the reaction. Meanwhile, O10 of the other H_2O molecule interacts with H8 and O7 in the five-membered-ring structure to form an O–H–O hydrogen bond.

② IM2 first passes through TS8 to form *trans*-N_2O_4–$2H_2O$. Both H_2O molecules are involved in the reaction course, and the product *trans*-N_2O_4–$2H_2O$ has an eight-membered-ring structure. Upon further reaction of *trans*-N_2O_4–$2H_2O$, the final product is formed through TS10. During this process, both H_2O molecules engage in proton-transfer phenomena, *i.e.*, O7 and

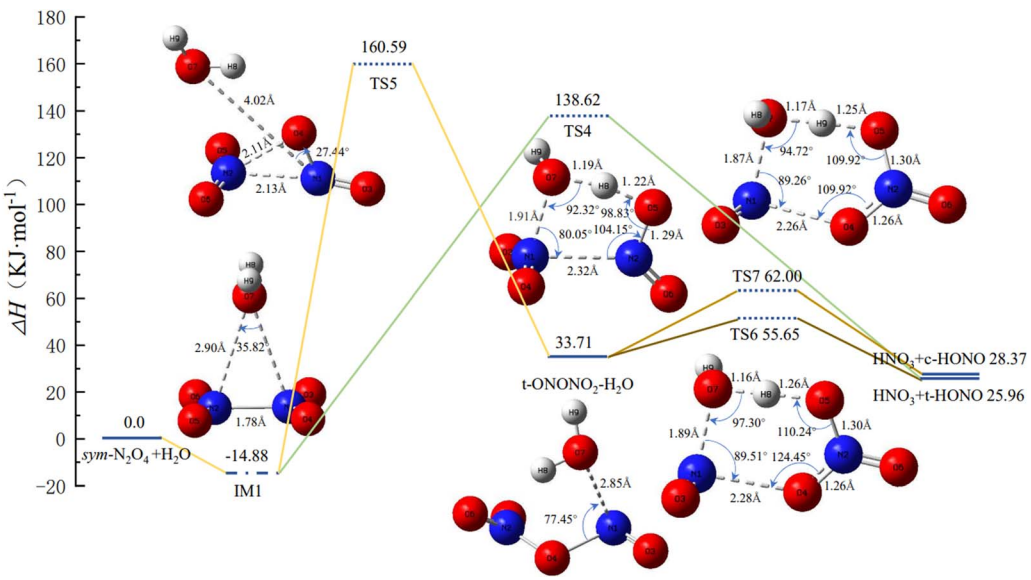

Fig. 2 Potential energy surface of $N_2O_4(H_2O)$ isomerization and reaction process, and the geometries and bond parameters of molecules (key length unit: Å, key angle unit: °).

Open Access Article. Published on 21 April 2023. Downloaded on 12/6/2025 3:27:13 PM.
This article is licensed under a Creative Commons Attribution-NonCommercial 3.0 Unported Licence.

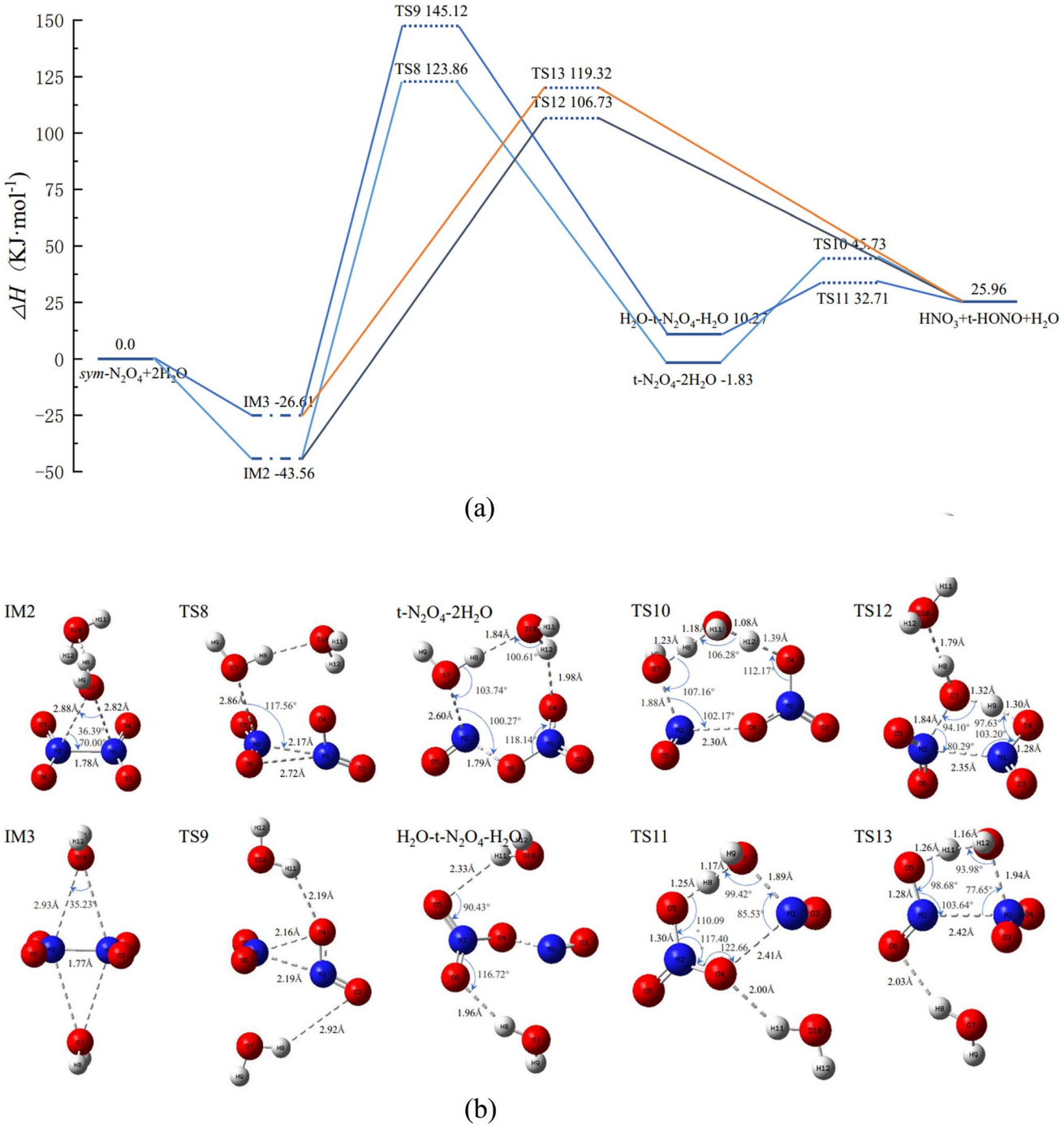

Fig. 3 (a) PES of $N_2O_4(H_2O)_2$ isomerization and reaction course. (b) Molecular geometrical configurations and bond parameters for N_2O_4–$(H_2O)_2$ isomerization and reaction course (bond lengths in Å, bond angles in °).

H10 of one H_2O molecule combine with NO to form *trans*-HONO, while H12 of the other H_2O molecule combines with NO_3^- to form HNO_3. The remaining H8 and O10 of the two H_2O molecules recombine with H11 to form a new H_2O molecule.

3.2.2 IM3 reaction process. ① IM3 undergoes a direct reaction *via* TS13 to form HNO_3 + *trans*-HONO + H_2O. The two H_2O molecules of IM3 in the steady state are symmetrically distributed on the upper and lower sides of N_2O_4, forming four N–O bonds, which are longer than the N–O bonds in IM2. Hence, IM3 is higher in energy than IM2. Upon isomerization of IM3, the H_2O molecule on one side resides closer to N_2O_4 after rotating through a certain angle about the N–N bond, and can participate in the reaction. At this point, TS13 also adopts a five-membered-ring structure. Compared with TS12, only the atoms connected to H_2O (O7), which is free from the five-membered-ring structure, are different. H9 of H_2O (O7) in TS13 is connected to O6 of one of the $-NO_2$ groups, forming a stable TS structure.

© 2023 The Author(s). Published by the Royal Society of Chemistry

Open Access Article. Published on 21 April 2023. Downloaded on 12/6/2025 3:27:13 PM.
This article is licensed under a Creative Commons Attribution-NonCommercial 3.0 Unported Licence.

② IM3 can also go through TS9 to first form H_2O–*trans*-N_2O_4–H_2O, and then O7 of H_2O, which is closer to N1, binds to N1 to form the six-membered-ring structure TS11. The latter is lower in energy and more stable than the eight-membered-ring structure of TS10. Of the H_2O (O7) molecule involved in the reaction, H8 combines with NO_3 to form HNO_3, while O7 and H9 combine with NO to form *trans*-HONO.

3.3 Isomerization and reaction profile of $N_2O_4(H_2O)_3$ ($n = 3$)

In $N_2O_4(H_2O)_3$, there are two possible distributions of H_2O molecules, *i.e.*, all three H_2O molecules residing on one side of N_2O_4, or two H_2O molecules on one side and the third on the other side. Our calculations reveal that N_2O_4–$3H_2O$ is lower in energy than $2H_2O$–N_2O_4–H_2O. Combined with the results in Section 3.2, $2H_2O$–N_2O_4–H_2O can be studied with reference to the isomerization and reaction profiles of IM2 and IM3, and so this section focuses on the isomerization and reaction profiles of N_2O_4–$3H_2O$, for which the PES and the geometric configurations and bond parameters of the molecules are shown in Fig. 4.

(1) IM4 may directly generate HNO_3 + *trans*-HONO + $2H_2O$ *via* TS16. In IM4, the three H_2O molecules are connected sequentially to form a ring structure with one of the $-NO_2$ groups, while O10 of the H_2O molecule located above N_2O_4 forms a stable triangular structure with both N atoms. The two N–O bonds are almost equal in length. Although only one H_2O molecule is involved in the reaction, H_2O (O10), in TS16 it forms both an eight-membered-ring structure with the remaining two H_2O molecules and a five-membered-ring structure with N_2O_4.

(2) IM4 first forms *trans*-N_2O_4–$3H_2O$ *via* TS14, and the three H_2O molecules also break from the ring structure into a single chain and then rejoin with O3 to form a ring. The *trans*-N_2O_4–$3H_2O$ then undergoes proton transfer, with H_2O (O7) providing –OH and H_2O (O10) providing H to form IM5. IM5 already has the structure of the products, but the molecules are still connected to each other and only form the products after bond-breaking.

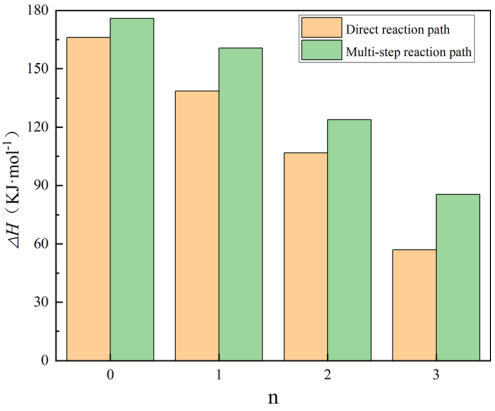

Fig. 5 Potential energy barriers associated with different reaction paths for $N_2O_4(H_2O)_n$ isomerization reactions.

$N_2O_4(H_2O)_n$ has one and only one stable structure during the isomerization and reaction course when $n < 2$. When $n \geq 2$, the distribution of H_2O affects the stable structure of $N_2O_4(H_2O)_n$, resulting in different energies. If H_2O is distributed on the same side of N_2O_4, with fewer interconnected chemical bonds and shorter bond lengths, the energy is lower and the structure is more stable, as in IM2 and IM3 in Fig. 3(b). Irrespective of whether n is odd or even, multiple pathways are available for $N_2O_4(H_2O)_n$ to undergo isomerization reactions. To verify the speculation of Miller *et al.*,[4] the potential energy barriers associated with different pathways of $N_2O_4(H_2O)_n$ isomerization for different values of n and pertaining to the most stable conformation are plotted in Fig. 5.

The energy of 166.01 kJ mol^{-1} for $n = 0$, *i.e.*, the direct ionization of N_2O_4 to form NO + NO_3, and combining TS4, TS12, and TS16 as the reaction potential for the direct reaction of $N_2O_4(H_2O)_n$ to form the product pathway; the first step of isomerization process of $N_2O_4(H_2O)_n$ through multiple steps to generate products as the reaction potential of its multi-step reaction pathway, *i.e.*, $N_2O_4(H_2O)_n \rightarrow$ *trans*-N_2O_4–$(H_2O)_n$: TS3, TS5, TS8, and TS14. From Fig. 5, it can be seen that the potential

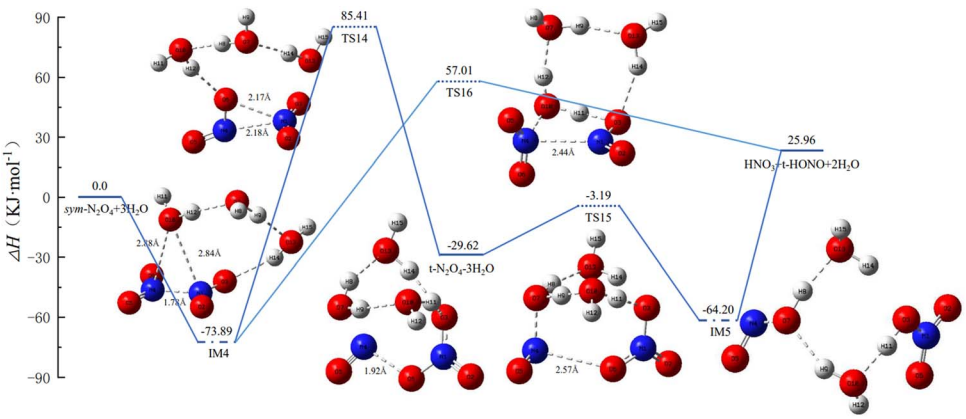

Fig. 4 Potential energy surface of $N_2O_4(H_2O)_3$ isomerization and reaction process, and the geometries and bond parameters of molecules (key length unit: Å, key angle unit: °).

Open Access Article. Published on 21 April 2023. Downloaded on 12/6/2025 3:27:13 PM. This article is licensed under a Creative Commons Attribution-NonCommercial 3.0 Unported Licence.

Table 1 Variations in charge on the *trans*-$ONONO_2$ group and ON–ONO_2 bond length in *trans*-$ONONO_2$–$(H_2O)_n$

n	0	1	2	3
Electric charge/a.u.	0	−0.019	−0.025	−0.503
Key length/Å	1.62	1.76	1.79	2.57

energy barrier of $N_2O_4(H_2O)_n$ gradually decreases as n is increased and more H_2O is involved in the reaction. When n = 0–2, the differences in the potential energy barriers associated with the direct and multi-step reaction paths are small, such that $N_2O_4(H_2O)_n$ may follow both reaction paths at the same time. When $n = 3$, however, the difference in potential energy barriers associated with the two paths reaches 28.4 kJ mol^{-1}, indicating that $N_2O_4(H_2O)_3$ will preferentially pass through TS16 to afford the products directly. Combined with the finding in Fig. 4 that TS15 is lower in energy than the reaction potential of the products when $N_2O_4(H_2O)_3$ undergoes a multi-step reaction path, it is clear that the multi-step reaction path of N_2O_4–$(H_2O)_3$ is difficult to reach. On the basis of thermodynamics, Mulliken charge analysis was performed on the intermediate product *trans*-$ONONO_2$–$(H_2O)_n$, and the results in terms of charge on the *trans*-$ONONO_2$ group and ON–ONO_2 bond length are shown in Table 1.

As can be seen from Table 1, the charge on the *trans*-$ONONO_2$ group gradually becomes more negative as the H_2O content in *trans*-$ONONO_2$–$(H_2O)_n$ is increased, indicating increased polarity. Concomitantly, the bond length of ON–ONO_2 also increases, and –ON gradually dissociates and from the *trans*-$ONONO_2$ group. It can be seen that the differences in charge on the *trans*-$ONONO_2$ group and ON–ONO_2 bond length are not large when $n = 1$ and 2. However, when $n = 3$, the charge on the *trans*-$ONONO_2$ group and the ON–ONO_2 bond length change abruptly, reaching −0.503 a.u. and 2.57 Å, respectively. These results support the conjecture of Miller *et al.*;[4] when $n = 1$ or 2, *trans*-$ONONO_2$-$(H_2O)_n$ is partly ionically bonded, but still mainly covalently bonded. When $n = 3$, however, ionic bonding becomes dominant. Meanwhile, combined with the reaction rate results of Miller *et al.*[4] and analyzed by the potential energy surfaces in Fig. 2–4, the reaction rate constant increases by two orders of magnitude when $n = 3$ compared with $n < 3$. In Section 3.2.1, *trans*-N_2O_4–$2H_2O$ was seen to undergo a proton-transfer phenomenon as the reaction proceeds. Luo *et al.*[14] confirmed that the formation of hydrogen bonds and a polar environment are prerequisites for intermolecular proton transfer. Proton-transfer due to *trans*-$ONONO_2$ dominates in the production of –OH, which is also supported by experimental results,[23] leading to a shorter lifetime of *trans*-$ONONO_2$ with the increase of H_2O. All charge-transfer steps result in partial reverse charge-transfer from NO_3^- to NO^+, making the ON–ONO_2 bond less susceptible to cleavage, further verifying that when $n = 3$, the $N_2O_4(H_2O)_3$ system is dominated by ionic bonds between molecules. Due to the short-lived existence of *trans*-$ONONO_2$ and the difficulty of breaking the ON–ONO_2 bond, the reaction can be considered as being completed instantaneously.[24] That is to say, IM4 mainly passes through TS16 to directly generate the final products HNO_3 + *trans*-HONO + $2H_2O$.

4 Conclusions

(1) $N_2O_4(H_2O)_n$ system structure reaction course of the local minimum is not related to the parity of the n value. When H_2O molecules are distributed on the same side, the potential energy of the system is lower, and the structure is more stable. When n = 1 or 2, the two reaction pathways are similar in energy. The systems are partly ionically bonded, but mainly still covalently bonded.

(2) When $n = 3$, the charge on the *trans*-$ONONO_2$ group and the ON–ONO_2 bond length change abruptly, reaching −0.503 a.u. and 2.57 Å, respectively, and the system is then dominated by ionic bonds.

(3) When $n = 2$, the reaction course shows the phenomenon of proton-transfer, with partial reverse charge-transfer from NO_3^- to NO^+, making cleavage of the ON–ONO_2 bond more difficult. Combining the change of potential energy surface, the charge on the $ONONO_2$ group, and the molecular bond parameters during the course of the reaction, it is again verified that $N_2O_4(H_2O)_n$ tends to afford the products directly in one step with increasing H_2O content in the system.

Author contributions

Y. Guo: conceptualization, investigation, methodology, writing – original draft. Z. Y. Huang: data curation, formal analysis. G. Tian: project administration, validation. W. Wu: resources, supervision. J. Lin: software, validation. X. L. Chang: funding acquisition, writing – review & editing.

Conflicts of interest

We declare that we do not have any commercial or associative interest that represents a conflict of interest in connection with the work.

Acknowledgements

This research was funded by the National Natural Science Foundation of China (No. 52272446) and Natural Science Foundation of Shaanxi Province (No. 2021JM-250).

References

1 Y. Guo, X. L. Chang, G. Tian, D. J. Liu and C. Pang, *Rare Met. Mater. Eng.*, 2022, **51**, 3459–3465.
2 D. J. Liu, G. Tian, Z. W. Yang, G. F. Jin, W. Zhang, Y. Wang and H. L. Wei, *Chin. J. Aeronaut.*, 2022, **36**, 304–315.
3 W. G. Liu and A. G. William, *J. Am. Chem. Soc.*, 2012, **134**, 12970–12978.
4 Y. Miller, B. J. Finlayson-Pitts and R. B. Gerber, *J. Am. Chem. Soc.*, 2009, **131**, 12180–12185.
5 A. S. Pimentel, C. A. L. Francisco and A. B. F. da Silva, *J. Phys. Chem. A*, 2007, **111**, 2913–2920.

© 2023 The Author(s). Published by the Royal Society of Chemistry

Open Access Article. Published on 21 April 2023. Downloaded on 12/6/2025 3:27:13 PM.
This article is licensed under a Creative Commons Attribution-NonCommercial 3.0 Unported Licence.

6 D. J. Medeiros and A. S. Pimentel, *J. Phys. Chem. A*, 2011, **115**, 6357–6365.
7 I. I. Zakharov, *Theor. Exp. Chem.*, 2012, **48**, 233–239.
8 R. S. Zhu, K. Y. Lai and M. C. Lin, *J. Phys. Chem. A*, 2012, **116**, 4466–4472.
9 R. Putikam and M. C. Lin, *Int. J. Quantum Chem.*, 2017, **118**, 25560–25569.
10 B. J. Finlayson-Pitts, L. M. Wingen, A. L. Sumner, D. Syomin and K. A. Ramazan, *Phys. Chem. Chem. Phys.*, 2003, **5**, 223.
11 T. C. Marilia, J. M. Anglada, J. S. Francisco and M. F. Ruiz-Lopez, *J. Am. Chem. Soc.*, 2020, **142**, 20937–20941.
12 F. Menezes and G. M. Popowicz, *Phys. Chem.*, 2022, **23**, 395.
13 Y. Miller and R. B. Gerber, *Phys. Chem. Chem. Phys.*, 2008, **10**, 1091–1093.
14 G. F. Luo and X. B. Chen, *J. Phys. Chem. Lett.*, 2012, **3**, 1147–1153.
15 J. S. Zhao, Z. Y. Huang, G. F. Jin, M. N. Gao and H. X. Zhu, *Chin. J. Energ. Mater.*, 2021, **29**, 1125–1131.
16 M. J. Frisch, G. W. Trucks, H. B. Schlegel, G. E. Scuseria, M. A. Robb, J. R. Cheeseman, G. Scalmani, V. Barone, G. A. Petersson, H. Nakatsuji, X. Li, M. Caricato, A. V. Marenich, J. Bloino, B. G. Janesko, R. Gomperts, B. Mennucci, H. P. Hratchian, J. V. Ortiz, A. F. Izmaylov, J. L. Sonnenberg, D. Williams-Young, F. Ding, F. Lipparini, F. Egidi, J. Goings, B. Peng, A. Petrone, T. Henderson, D. Ranasinghe, V. G. Zakrzewski, J. Gao, N. Rega, G. Zheng, W. Liang, M. Hada, M. Ehara, K. Toyota, R. Fukuda, J. Hasegawa, M. Ishida, T. Nakajima, Y. Honda, O. Kitao, H. Nakai, T. Vreven, K. Throssell, J. A. Montgomery Jr, J. E. Peralta, F. Ogliaro, M. J. Bearpark, J. J. Heyd, E. N. Brothers, K. N. Kudin, V. N. Staroverov, T. A. Keith, R. Kobayashi, J. Normand, K. Raghavachari, A. P. Rendell, J. C. Burant, S. S. Iyengar, J. Tomasi, M. Cossi, J. M. Millam, M. Klene, C. Adamo, R. Cammi, J. W. Ochterski, R. L. Martin, K. Morokuma, O. Farkas, J. B. Foresman, and D. J. Fox, *Gaussian 16, Revision A.03*, Gaussian, Inc., Wallingford CT, 2016.
17 A. Givan and A. Loewenschuss, *J. Chem. Phys.*, 1989, **90**, 6135.
18 A. Givan and A. Loewenschuss, *J. Chem. Phys.*, 1989, **91**, 5126.
19 A. Givan and A. Loewenschuss, *J. Chem. Phys.*, 1991, **94**, 7562.
20 B. W. McClelland, G. Gundersen and K. Hedlberg, *J. Chem. Phys.*, 1972, **56**, 4541.
21 K. Y. Lai, MS thesis, National Chiao Tung University, Taiwan, 2009.
22 A. Chou, R. Zhi and F. M. Tao, *J. Phys. Chem. A*, 1999, **103**, 7848.
23 T. Kinugawa, S. Enami, A. Yabushita, M. Kawasaki, M. Hoffmann and A. Colussi, *Phys. Chem. Chem. Phys.*, 2011, **13**, 5144–5149.
24 A. Yabushita, S. Enami, Y. Sakamoto and M. Kawasaki, *J. Phys. Chem. A*, 2009, **113**, 4844–4848.

© 2023 The Author(s). Published by the Royal Society of Chemistry